Analytica Chimica Acta 761 (2013) 84–91

Contents lists available at SciVerse ScienceDirect

Analytica Chimica Acta

journal homepage: www.elsevier.com/locate/aca

Redox-active thionine–graphene oxide hybrid nanosheet: One-pot, rapid synthesis, and application as a sensing platform for uric acid

Zhoumin Sun, Haiying Fu, Liu Deng*, Jianxiu Wang

Key Laboratory of Resources Chemistry of Nonferrous Metals, Ministry of Education, College of Chemistry and Chemical Engineering, Central South University, Changsha 410083, Hunan, People's Republic of China

HIGHLIGHTS

- A simple wet-chemical strategy for synthesis of thionine–graphene oxide hybrid nanosheets (T–GOs).
- T–GOs serve as a biocompatible matrix for enzyme assembly and a mediator.
- A simple and effective sensor for assay of uric acid at physiological levels. ► Demonstrate further application of GOs for biosensors and other fields.

GRAPHICAL ABSTRACT

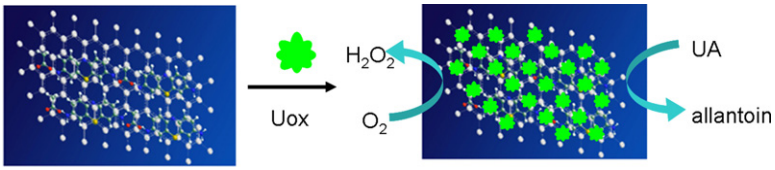

ARTICLE INFO

Article history:
Received 25 October 2012
Received in revised form
26 November 2012
Accepted 28 November 2012
Available online 5 December 2012

Keywords:
Graphene oxide
Thionine
Hybrid nanosheets
Uric acid
Biosensor

ABSTRACT

In this paper, we fabricate a sensitive and stable amperometric UA amperometric biosensor using nanobiocomposite derived from thionine modified graphene oxide in this study. A simple wet-chemical strategy for synthesis of thionine–graphene oxide hybrid nanosheets (T–GOs) through π–π stacking has been demonstrated. Various techniques, such as UV–vis absorption spectroscopy, X-ray photoelectron spectroscopy (XPS), transmission electron microscopy (TEM), atomic force microscopy (AFM) and electrochemistry have been utilized to characterize the formation of the T–GOs. Due to the synergistic effect between thionine and graphene oxide, the nanosheets exhibited excellent performance toward H_2O_2 reduction. The incorporation of thionine onto graphene oxide surface resulted in more than a twice increase in the amperometric response to H_2O_2 of the thionine modified electrode. The as-formed T–GOs also served as a biocompatible matrix for enzyme assembly and a mediator to facilitate the electron transfer between the enzyme and the electrode. Using UOx as a model system, we have developed a simple and effective sensing platform for assay of uric acid at physiological levels. UA has been successfully detected at −0.1 V without any interference due to other electroactive compounds at physiological levels of glucose (5 mM), ascorbic acid (0.1 mM), noradrenalin (0.1 mM), and dopamine (0.1 mM). The response displays a good linear range from 0.02 to 4.5 mM with detection limit 7 μM. The application of this modified electrode in blood and urine UA exhibited a good performance. The robust and advanced hybrid materials might hold great promise in biosensing, energy conversion, and biomedical and electronic systems.

1. Introduction

Uric acid (UA) is the primary final product of endogenous purine derivatives in human metabolism. The concentration change of UA in body fluids might induce several pathological disorders, such as gouty arthritis, cardiovascular and neurological diseases, etc. [1–4]. Recent studies suggest that UA could act as an antioxidant to protect against oxidative damage by ROS (reactive oxygen species), or contribute significantly to the inflammatory responses in vivo induced by cell death [5,6]. In order to understand the clinical consequence of UA concentration alternation, a reliable, simple method for routine detection of UA is of great importance.

* Corresponding author.
E-mail address: dengliu@csu.edu.cn (L. Deng).

0003-2670/$ – see front matter © 2012 Elsevier B.V. All rights reserved.
http://dx.doi.org/10.1016/j.aca.2012.11.057

Due to its high sensitivity, simpleness, and suitability for miniaturization, electrochemistry is promising for determination of UA in biological media [7–14]. However, the electrochemical oxidation of UA is usually affected by interfering species [9,10]. Enzyme has a unique ability of molecular recognition, the development of enzyme-based electrochemical method, which is highly selective and sensitive, has attracted much attention. As we know, uricase (UOx) can catalyze the oxidation of UA in the presence of oxygen with the formation of CO_2 and H_2O_2, so quantification of UA can be achieved by measuring the concentration of the enzymatically generated H_2O_2. However, the potential for H_2O_2 oxidation is positive enough to cause direct oxidation of UA and other components, such as ascorbate and acetaminophen, resulting in inaccurate determinations [10]. To solve the problem, several attempts have been made to decrease the overpotential of H_2O_2 oxidation, such as the use of peroxidase [8] or redox mediator [9–11]. In recent years, nanomaterials have attracted growing attention for facilitating electron transfer kinetics for H_2O_2 determination [14–18]. For example, Pt–graphene nanosheets [10], ZnS quantum dots [14], ZnO nanowires and nanorods [15,16] and thionine-SWNT (single-wall carbon nanotube) hybrid [17] have been employed as a matrix for UOx immobilization and for UA assay. Graphene oxide (GO), a "rising star" material, has received considerable interest due to its unique properties, such as water dispersibility, versatility of surface modification, large specific surface area, and excellent mechanical, electrical, and thermal properties, thus making it a promising building block for nanoelectronics, energy storage/conversion, catalysis, and sensors [19–35]. For instance, field effect transistor (FET) biosensors based on graphene oxide or other graphene forms have been fabricated, which allowed sensitive detection of DNA, protein, and even bacterium or pH [36–39]. Direct electron transfer of glucose oxidase [40,41] or horseradish peroxidase (HRP) [42] was also realized on graphene modified electrode, which showed high electrocatalytic activity toward glucose [41] and H_2O_2 [42–44]. From the select examples, it is evident that noncovalent functionalization of GO through π–π stacking and hydrophobic interaction is of great interest because the intrinsic properties of GO are preserved. To explore further applications of GO, multifunctional materials combining the superior properties of GO with the functional molecules have been attempted. Thionine is an artificial organic dye derivative of phenothiazine. Due to its electroactive and photoactive properties, thionine has been widely utilized in photogalvanic cells and electrochemical biosensors [45].

In this paper, multifunctional material of thionine–graphene oxide nanosheets (T–GOs) has been fabricated and used for UA sensing. The synthesized T–GOs served as an electron mediator and a matrix for enzyme immobilization. The UOx–T–GOs exhibited excellent amperometric response to uric acid, holding great promise for clinical diagnosis of certain genetic diseases.

2. Experimental

2.1. Chemicals

Thionine, uric acid, glucose, ascorbic acid (AA), dopamine (DA), and noradrenalin (NE) were purchased from Sigma. Uricase (EC 1.7.3.3 from Baomanbio, lyophilized powder, approximately 12.5 units mg^{-1}) was purchased from Bio Basic Inc. Nafion (5% w/w solution) was obtained from Alfa Aesar. All other chemicals were of analytical grade. All solutions were prepared with double distilled water. 0.1 M phosphate buffered saline (PBS, pH 7.4), prepared from Na_2HPO_4 and NaH_2PO_4, was employed as the supporting electrolyte. Stock solution of 10 mM UA was prepared with 0.3 M NaOH, and then pH of the solution was adjusted to 7.4 using 1.0 M HCl.

2.2. Apparatus

AFM and TEM images were recorded on a Nanoscope IIIa scanning probe microscope (Digital Instruments, USA) with a tapping mode and on a JEOL-2010 transmission electron microscope operating at an accelerating voltage of 200 kV, respectively. XPS spectra were acquired on Thermo Fisher Scientific, K-Alpha 1063 spectrometer. The electrochemical determinations were performed with a CHI 900B electrochemical workstation (CH Instruments). A three-electrode system was employed in which a glassy carbon (GC) electrode, a coiled Pt wire and a saturated calomel electrode (SCE) were used as the working electrode, counter electrode and reference electrode, respectively. All electrochemical characterizations were performed at room temperature ($22 \pm 1\,^{\circ}C$).

2.3. Synthesis of thionine-functionalized graphene oxide nanosheets (T–GOs)

T–GOs were prepared as follows: 20 mL of 0.5 mg mL^{-1} homogeneous suspension of graphene oxide, synthesized from natural graphite by Hummers' method with little modification [31], was mixed with 20 mL of 0.2 mM thionine aqueous solution. After being vigorously shaken or stirred for 30 min, the stable dark green species was collected by centrifugation at 10,000 rpm for 20 min. The obtained T–GOs were washed at least three times with water to rid any loosely absorbed thionine molecules.

2.4. Preparation of T–GOs and UOx–T–GOs modified electrodes

Prior to modification, the GC electrode (3 mm in diameter) was polished sequentially with 1.0, 0.3 and 0.05 μm alumina slurry, followed by thoroughly rinsing the electrode with double distilled water between each polishing step. The above electrode was then successively washed with 1:1 nitric acid, acetone and double distilled water in ultrasonic bath and dried in air. The T–GOs modified electrode was prepared by casting 5 μL of 0.25 mg mL^{-1} T–GOs suspension on the GC electrode surface and then dried in air. Before fabrication of the UOx–T–GOs modified electrode, 100 μL of UOx (5 mg mL^{-1} in PBS, pH 7.4) was mixed with 100 μL of T–GOs suspension (0.25 mg mL^{-1}). After stirring for 5 min, 5 μL of the resultant mixture was assembled onto the GC electrode surface. The as-prepared UOx–T–GOs/GC electrode was stored at 4 °C and ready for use.

3. Results and discussion

3.1. The characterization of T–GOs hybrid nanosheets formation

Thionine, a small planar molecule, contains one heterocyclic nitrogen atom and two amine groups symmetrically distributed on each side. These interactions between amino groups of thionine and GOs, and π–π stacking force between GOs and thionine molecules, might account for thionine cross-linking GOs. UV–vis absorption spectrum was carried out to investigate the interaction between the thionine and the GO. As shown in Fig. 1A, the GO dispersion displays a maximum absorption at 228.5 nm which is due to the π–π^* transition of aromatic C=C bonds and a shoulder at 290–300 nm which corresponds to the n–π^*transition of the C—O bond. The diluted thionine aqueous solution has two characteristic absorption peaks, at 282 nm in far-ultraviolet region and at 560, 599 nm in visible light region, which correspond to the long wavelength π–π^* transitions of aromatic rings and the n–π^* transitions of C=N bond, respectively. The main peak at 599 nm is characteristic of monomeric thionine, while the 560 nm shoulder can be attributed to the T-type dimer aggregate. The T–GOs exhibit absorption at 228.5 nm which should be the corresponding

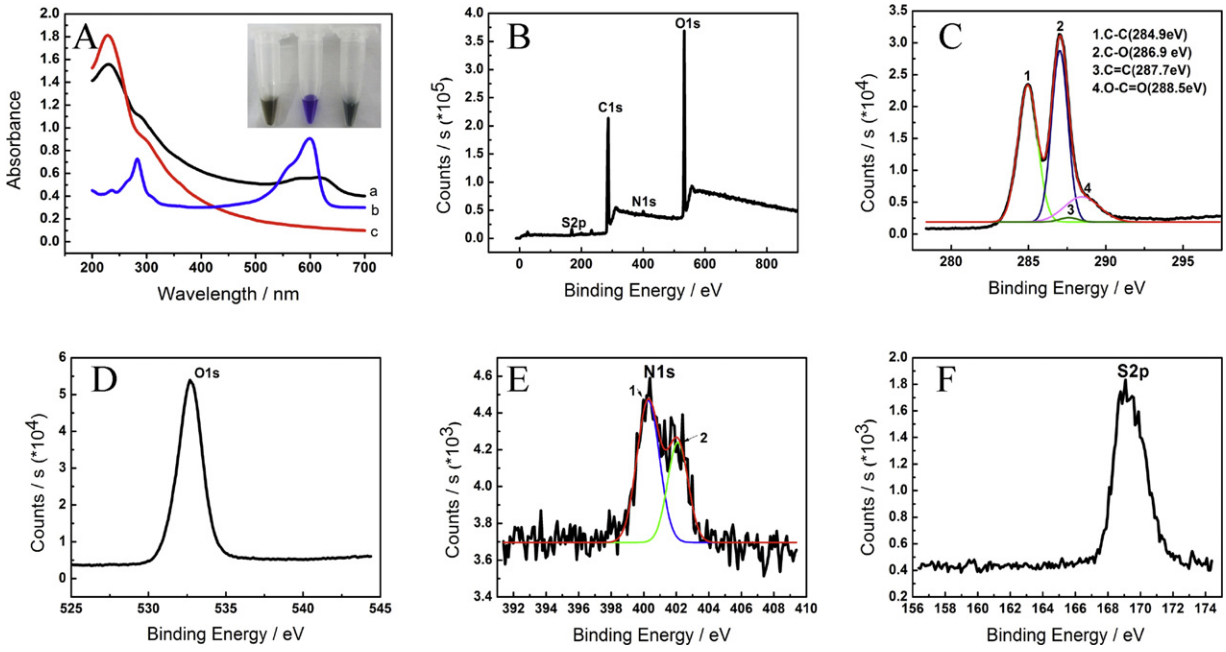

Fig. 1. (A) UV–vis spectra of T–GOs suspension (a), thionine solution (b), and GO suspension (c) inset: photographs of GO (a), thionine (b), and T–GOs (c) dispersion in water. XPS data for T–GOs (B). The deconvolution of C 1s spectra (C), O 1s spectra (D), N 1s spectra (E), S 2p spectra (F).

GO and suggests that the dimerization equilibrium is not significantly disrupted when thionine is adsorbed on GOs. The observed red shift is evidence of strong interaction between GOs and thionine molecules. This clearly confirms that thionine molecules are attached to GOs.

X-ray photoelectron spectroscopy (XPS) was employed to further explore the interactions between GO and thionine. The survey of T–GOs (Fig. 1B) shows the presence of N1s and S2p originating from thionine. Elemental analysis was carried out to obtain the compositions of C, O, N and S elements in the T–GOs nanosheets. The high-resolution XPS spectrum of the C 1s region is illustrated in Fig. 1C. The deconvolution of C 1s spectrum indicated the presence of four types of carbon bonds: C—C (284.6 eV), C—O (286.7 eV), C═O (287.8 eV), and O—C═O (288.7 eV) [46]. The optimum curve fitting of the O 1s peak of the prepared carbon fibers is shown in Fig. 1D. The peak at 532.6 eV corresponds to the carbonyl oxygen atoms [47]. N 1s spectrum is obtained to identify the distribution of N functionalities (Fig. 1E). Two peak N 1s signals at 401.8 eV and 402.3 eV are due to amine NH_2 groups and to the nitrogen atoms in pyridine-N-oxides, respectively [45,48]. The S 2p signal (Fig. 1F) at 169.1 eV originated from S—N bond in thionine molecule [45]. These results indicate that the noncovalent functionalization of graphene oxide by thionine successfully occurred.

TEM image of a sheet of the T–GOs (Fig. 2A) clearly shows an ultra-thin paper like wrinkled morphology. Thionine, a small planar molecule, contains one heterocyclic nitrogen atom and two amine groups symmetrically distributed on each side. Its amine groups possess high binding affinity for GO via amine–carbonyl interaction. Also, there is π–π stacking force between GOs and thionine molecules. These interactions might account for thionine functionalized GO. The morphology and thickness of T–GOs have also been studied by AFM observation. The AFM image of Fig. 2B and the corresponding sectional analysis demonstrate that the thickness of T–GOs is about 1.4 nm, which is thicker than unmodified graphene oxide. The thickness of the typical single-layer grapheme oxide sheets is about 1.08 nm. The average thickness of T–GOs is determined to be about 1.46 nm. There was 0.38 nm increment compared with that of unmodified GO, owing to the presence of thionine on the GO sheet surfaces. Since thionine could locate on both sides of the GO, the thickness of thionine layer on GO was calculated to be about 0.16 nm. This data was consistent with the thickness of a single thionine molecule (0.11 nm) [43]. So we assumed that GO nanosheets were covered by a monolayer of thionine. The uniform nanostructure can significantly increase the effective surface of the electrode for loading of biomolecules and accelerating electron transfer rate. In the present study, UOx is negatively charged in pH 7.0 because its isoelectric point is 5.4. A zeta potential value of 25.6 mV of the as-prepared T–GOs was measured. Thus, the T–GOs could act as electrostatic anchor for absorption of positively charged UOx through the self-assemble methodology. The assembly of UOx on the T–GOs surface is further confirmed by the TEM images (Fig. 2C) UOx molecules were aggregated on T–GOs due to the large surface-to-volume ratio of GOs. As a result, the T–GOs nanosheets become "thick". After UOx was assembled on the surface of the T–GOs, many cracks and high surface roughness appear. These nanostructures are the aggregates of UOx molecules, indicating that the enzyme has been effectively immobilized on the surface of T–GOs. And these distributed island-like nanostructures implied that the novel composites could increase the electroactive surface area of the T–GOs electrode. Such a structure is expected to be very attractive for the detection of substrates because each of the hybrids is fully and easily accessible to substrates and, therefore, can be used as an electrochemical sensing unit, yielding a high ratio of signal-to-noise for electrochemical determination.

3.2. Electrochemical properties of T–GOs/GC electrodes

Further support for the formation of T–GOs hybrid nanosheets can be provided by electrochemistry characterization. Fig. 3A shows typical cyclic voltammograms (CVs) obtained at the T–GOs modified GC electrode at various scan rates in PBS (pH 7.4) solution. This redox wave at formal potential ca. −0.25 V is ascribed to oxidation/reduction of thionine. The value of E^0 is 57 mV more negative than the original thionine modified GC in the same electrolyte. This is probably due to some thionine redox centers attached on the GO surface by the interaction of π–π stacking, this electron-drawing

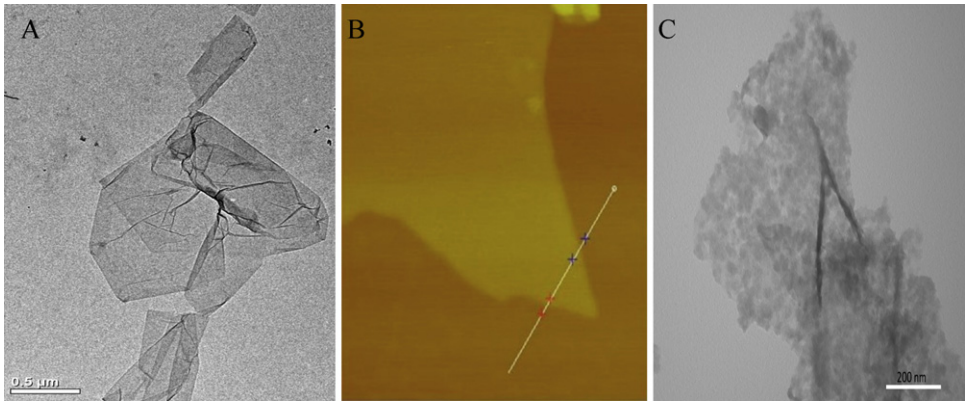

Fig. 2. (A) TEM image of T–GOs nanosheets. (B) AFM images and the cross-sectional analysis of GO sheets with assembly of thionine. (C) TEM image of UOx–T–GOs.

effect results in the negative shift of E^0. While an electrostatic Donnan effect may also ascribe to this phenomenon.

It is noted that the T–GOs show very good redox reversibility with peak-to-peak separations being around 30 mV. The results show that thionine molecules may electrically communicate to each other due to the well-known interpenetration phenomenon within the GO surface that allows an electron hopping process between adjacent redox groups. The ΔE_p of for T–GOs/GC exhibited larger than that of thionine/GC (ca. 21 mV at 50 mV s^{-1}), suggesting that the interactions between GO and thionine facilitate the electron transfer from thionine toward electrode surface. The reversibility of the voltammetric responses in aqueous solution for the T–GOs nanosheets is highly improved, as compared with those of other thionine nanomaterials [46–48].

The modified electrode shows the characteristic of chemically reversible surface redox electrochemistry. A plot of the cathodic peak current as a function of scan rate is linear up to 800 mV s^{-1} (the inset of Fig. 3B). Also, the formal potentials are independent of scan rates and the cathodic and anodic peak currents ratio is unity at all scan rates. All of these demonstrate that the redox processes of surface confined thionine are fast from the underlying substrate to T–GOs nanosheets. Based on the above-mentioned result that an equal amount of thionine was deposited in each deposition step, the average surface coverage for the thionine molecules on GO surface is estimated to be 0.66095×10^{-7} mol g^{-1}. In addition, the T–GOs modified electrode was found to be extremely stable during the whole electrochemical measurement even when continuous cycling between −0.6 and 0.2 V for 1 h. This facile electron accessibility and good stability of the as-prepared T–GOs offered the possibility for electrochemical catalysis.

3.3. Electrochemical reduction of H_2O_2 at the T–GOs/GC electrode

A detailed study of the electrocatalytic behavior toward H_2O_2 reduction on the T–GOs/GC electrode was carried out in this section. To discern the contribution of individual components and the possible synergistic effect among them, control experiments on bare GC, GO/GC, Th/GC, T–GOs electrodes were also carried. As shown by the cyclic voltammograms in Fig. 4, the bare GC and T–GOs/GC electrodes exhibit similar electrocatalytic activity toward the reduction of H_2O_2. The electrochemical reduction of H_2O_2 on the bare GC electrode starts at −0.08 V, while this reaction on the GOs/GC electrode occurs at −0.10 V. There is slight negative shift of the onset potential for the reduction of H_2O_2 on the GOs/GC electrode. However, the reduction current is larger than that on the bare GC electrode. In previous reports, GO possess intrinsic peroxidase property, which would play as mimic enzymes catalysis to improve the response toward H_2O_2 reduction. In addition, the increased surface area also plays an important role in the observed increased current.

At the same time, the thionine modified electrode shows much better electrocatalytic activity. As shown in Fig. 4C, this Th/GC electrode displays the typical redox characteristics of thionine. The electrochemical reduction of H_2O_2 already starts at −0.05 V, which is about a 30 mV positive shift of the onset potential as compared to the bare GC electrode. This onset potential is consistent with that for the reduction of thionine, indicating that thionine is a good electron mediator for the H_2O_2 reduction. This result is in good agreement with those observed previously [48–50]. At about −0.2 V, a maximum reduction current of 2.5 μA is observed, and at more negative potentials, the cathodic current shows a plateau. Shown in Fig. 4D, curve a is CVs of the T–GOs/GC electrode in PBS (pH 7.4) without H_2O_2 in N_2 atmosphere. In the presence of

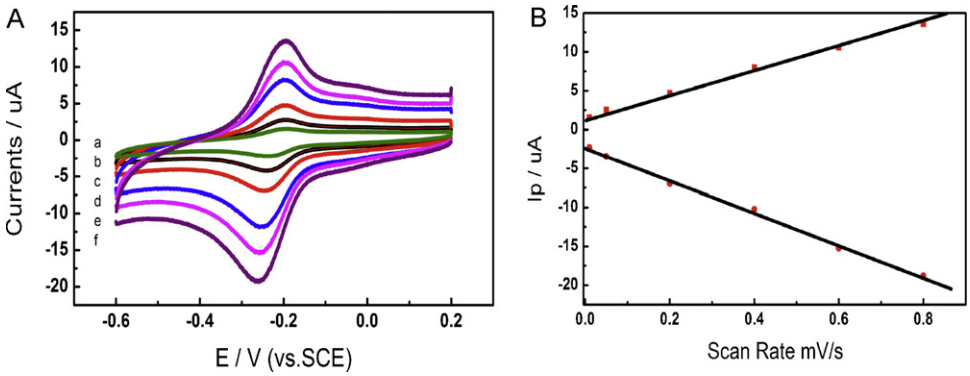

Fig. 3. (A) Voltammetric response of the T–GOs electrode in N_2-saturated PBS (0.1 M, pH 7.4) at different scan rate of 10 mV s^{-1} (a), 50 mV s^{-1} (b), 200 mV s^{-1} (c), 400 mV s^{-1} (d), 600 mV s^{-1} (e), 800 mV s^{-1} (f). (B) Shows dependence of peak currents on scan rates for the T–GOs/GC electrode.

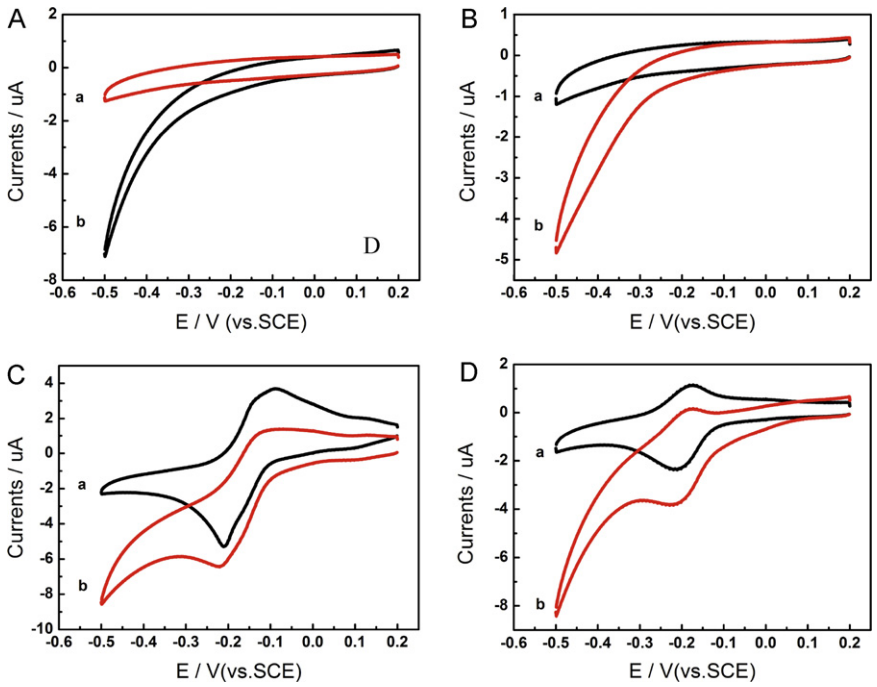

Fig. 4. Voltammetric responses of the bare GC (A), GO/GC (B), Th/GC (C) and T–GOs (D) electrodes in N_2-saturated PBS (0.1 M, pH 7.4) with (curve b) and without (curve a) 5 mM H_2O_2. Scan rate is 50 mV s^{-1}.

H_2O_2, a remarkable catalytic reduction current at the modified electrode occurred at ca. −30 mV. When thionine was incorporated in the T–GOs/GC electrode, a cathodic current twice as large as that of the Th/GC electrode is observed, and the onset potential is only slight positive shift. The onset potential for H_2O_2 reduction on this T–GOs/GC electrode appears as the most positive value amongst all of these electrodes. These results demonstrated that the T–GOs/GC electrode exhibited the best response toward electrochemical reduction of H_2O_2.

Fig. 5 shows the amperometric response to the successive addition of H_2O_2 in pH 7.4 PBS at the T–GOs composite modified electrode electrode at −0.25 V. The current response displayed a linear range from 50 μm to 11.2 mM with detection limit of 18 μM. The electrochemical results demonstrate that the T–GOs composite modified electrode maintains the good electrochemical activity of H_2O_2 and could find applications in the field of electrochemistry.

The increased cathodic current on the T–GOs composite film electrode cannot be due to the assembled thionine on GO surface but should be due to the synergistic effects between the GO nanosheets and thionine molecular because the current $I_{(T\text{–}GOs)} \gg (I_{GO} + I_{Th})$, where $I_{(T\text{–}GOs)}$ is the current due to the reduction of H_2O_2 at the T–GOs/GC electrode, and I_{GO} and I_{Th} are the reduction currents of H_2O_2 at GO and thionine-modified GC electrodes, respectively. Such synergy has been recently observed by several groups in their study of the electrocatalytical small biomolecules on the CNTs and redox mediators integrated system [51–56]. These authors explained the observed synergy by the hypothesis that the introduction of redox mediators into the CNTs matrix improved mediator electronic and ionic transport capacity and electron self-exchange in the polymer film. This hypothesis can also be applied to T–GOs hybrid nanosheets. Using T–GO nanosheets as the enzyme matrix have several advantages for biosensing applications. Due to its highly conductivity, biocompatibility, cheap and low cytotoxicity, T–GO is an ideal functional material for electrochemical analysis. Second, there are ubiquitous corrugations on T–GO nanosheets, and the resulting layered enzyme-T–GO nanocomposites would have interlayer spacing to facilitate the mass transport. Third, the thionine assembled on GO surface can be applied as an efficient mediator to facilitate the electron transfer through the enzyme toward electrode surface.

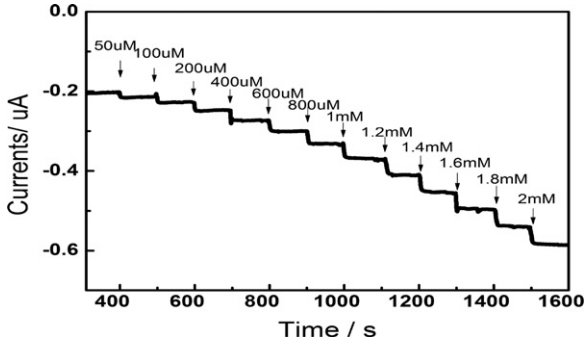

Fig. 5. The hydrodynamic responses of a T–GOs composite modified GC electrode at a detection potential of −0.25 V vs. SCE in a stirred phosphate buffer solution (pH 7.4) upon continuous injection of different concentration H_2O_2 for each step.

3.4. UOx–T–GOs based biosensor for uric acid detection

To verify the prepared T–GOs hybrid nanosheets can act as a platform for enzyme biosensor fabrication, the biosensor was prepared by incorporating a model enzyme UOx into the T–GOs. The UOx catalyzes, in the presence of oxygen, the oxidation of UA to allantoin, producing H_2O_2 simultaneously. Then the enzymatically generated H_2O_2 can be measured based on its reduction that occurred at T–GO nanosheets surface. Thus, the UA concentration can be measured by the current for electrochemical reduction of H_2O_2. The electrocatalytic processes that occurred at the electrode surface can be depicted as the following:

$$UA + O_2 \xrightarrow{UOx} \text{allantoin} + H_2O_2 + CO_2 \quad (1)$$

$$H_2O_2 + \text{thionine(Red)} \rightarrow 2H_2O + \text{thionine(Ox)} \quad (2)$$

$$\text{Thionine(Ox)} + H^+ + 2e \rightarrow \text{thionine(Red)} \quad (3)$$

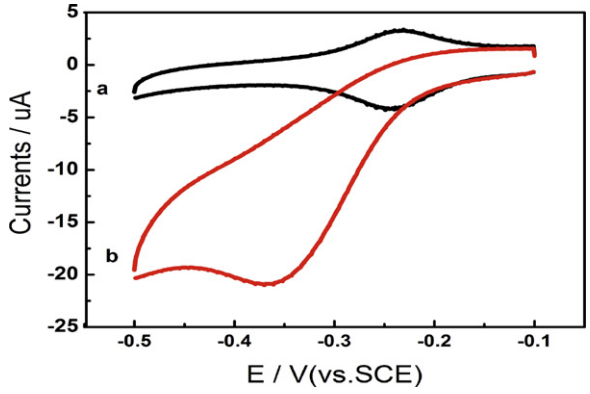

Fig. 6. Cyclic voltammograms of the UOx–T–GOs/GC electrode in air-saturated PBS with (b) and without (a) 5 mM UA. The scan rate is 10 mV s^{-1}.

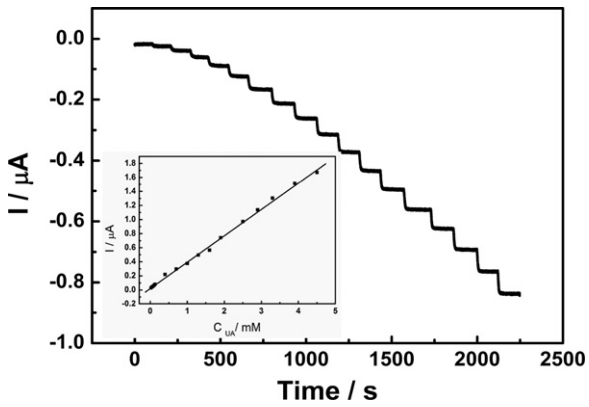

Fig. 8. The hydrodynamic responses of a T–GOs composite modified GC electrode at a detection potential of −0.25 V vs. SCE in a stirred phosphate buffer solution (pH 7.4) upon continuous injection of different concentration UA for each step. Inset: the calibration curve of the T–GOs composite modified GC electrode toward UA.

Here, the electrocatalytic activity of the UOx–T–GOs hybrid nanosheets toward uric acid was investigated. UOx–T–GOs/GC electrode shows a pair of redox peaks with the peak potential and currents almost identical with those of T–GOs/GC electrode (Fig. 6), demonstrating that assembly of the enzyme does not affect the electrochemical characteristics of T–GOs. This feature is important for T–GOs being utilized as a useful mediator after it was immobilized on the electrode surface with an enzyme. Upon addition of 5 mM UA, a rapid increase in the cathodic current appears as a result of the reduction of H_2O_2 produced from the enzymatic reaction. These results suggest that the UOx–T–GOs/GC electrode can be used as a biosensor to detect UA.

The solution pH has significant effects on the biosensor performance. In the pH range from 5 to 9, an optimal response is found at approximately pH 7–7.5 (Fig. 7A), which is in good agreement with that reported for the UOx dissolved in solution. This result indicates that the assembly procedure can keep the native activity of UOx. The response decreases significantly at a higher pH value. The detection potential is necessary to achieve the lowest detection limit and avoid the electrochemical interfering species. The responses of 0.1 mM UA at the UOx–T–GOs/GC electrode at different detection potentials from 0 to −500 mV were recorded. Basically, the response keeps on rising when the potential is moved from 0 to −250 mV and decays slightly after that potential. Moreover, a more negative potential leads to increase in noise. Thus, a detection potential of −250 mV is selected in this work. The low detection potential will significantly diminish the influence of those easily oxidizable species.

In real samples, there are some coexisting electroactive species such as glucose, AA, NE, DA, etc. that might affect the biosensor response. The selectivity and anti-interference advantages of the biosensor are demonstrated (Fig. 7B). A well-defined UA response is observed at the biosensor, whereas relevant physiological levels of glucose (5 mM), AA (0.1 mM), NE (0.1 mM), DA (0.1 mM) result in negligible signals. This feature is largely attributed to the use of a low operating potential in the detection. Therefore, highly selective response to UA is obtained without the use of a perm-selective membrane or enzymatic preoxidation. This is an advantage of the proposed biosensor over those reported previously. These results indicate the suitability of the proposed biosensor to practical applications.

Fig. 8 showed the steady-state responses of adding different amount of UA at an applied potential −0.25 V. The response of the sensor was rather fast typically within 10 s, suggesting that the electrode responds rapidly to the change of the UA concentration. The fast response may be majorly attributed to the fast diffusion of H_2O_2 in the open 3D architectures of the UOx–T–GOs hybrid nanosheets on the electrode and the synergistic catalytic effect of the T–GOs nanosheets toward H_2O_2. The response displays a good linear range from 0.02 to 8.5 mM with detection limit 7 μM. The detection limit is lower than that obtained at a UA biosensor based on polyaniline–UOx electrode [13]. The linear response range is wider than those of 4 μM–0.64 mM at polyaniline–UOx electrode [13] and 5–150 μM at UOx–DTB–PET/MPx-11 electrode [57]. UA normal level in serum ranges from 0.3 to 0.5 mM and in urinary excretion is typically 1.4–4.4 mM. This linear concentration range is suitable for the determination of UA level in blood and urine samples. These results suggest that graphene oxide can be

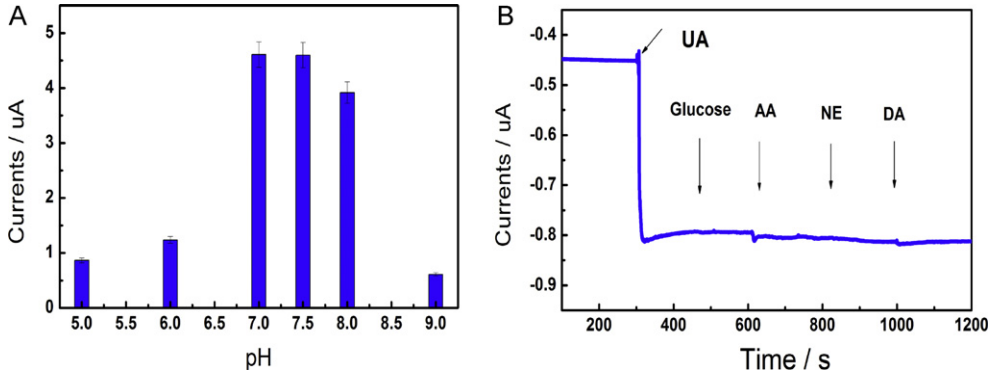

Fig. 7. (A) The dependence of the response of 1 mM UA at the UOx–Th–GO/GC electrode on the pH of the buffer. (B) The selectivity profile of the electrode over interfering species of glucose (5 mM), AA (0.1 mM), NE (0.1 mM), and DA (0.1 mM) obtained at applied potential of −250 mV vs. SCE. Every value is an average value of three independent measurements.

Table 1
Determination of uric acid in human blood and urine samples.

Sample	Biosensor (mM)	RSD (%)	Recovery (%)
Blood	0.22	2.75	99.6
	0.45	3.09	98.3
Urine	3.08	2.89	101.5
	4.22	3.26	103.2
	2.78	3.17	102.8

used as a biocompatible platform for development of UOx-based amperometric biosensors for UA determination.

The UOx–T–GOs electrode provides excellent catalytic performance for the detection of UA could ascribe to the following reasons. First, the nanostructure films generally have better catalytic efficiencies than the flat surface. There are many cracks on the UOx–T–GOs nanosheets surface, the channels between these cracks may allow counterions in aqueous buffers to move into or out of the films more easily and greatly enhance the charge transport mobility within the films. And the increased working electrode area provided by GOs allowed for more of the redox thionine centers to be accessible. Second, the T–GOs play a significant role in the enzyme immobilization as carriers for UOx to provide a suitable microenvironment to retain the UOx activity. T–GO nanosheets can provide 'flexible distance' and restack by adapting to the dimensions of the biomolecules, which is important to retain the enzyme native structures. Third, T–GOs acted as a transducer for amplifying the electrochemical signal of the product of the enzymatic reaction. Recent studies demonstrated that graphene could realize the direct electron transfer of enzymes at electrode surface. Here, the UOx may partially unfold when they associated with GO surface, which allowed for improved access to the active centers by the thionine redox centers.

The reproducibility and stability of the biosensor were evaluated. Six different UOx–T–GOs/GC electrodes were investigated in the current response to 2 mM UA. The results revealed that the biosensor has good reproducibility with a relative standard deviation (RSD) of 3.6%. In addition, a set of 10 different amperometric measurements for 2 mM UA at −0.25 V with a single biosensor yielded an RSD of 2.6%, indicating good repeatability of the measurements. To illustrate feasibility of the fabricated UA biosensor in practical analysis, the UOx–T–GOs/GC electrode was used to detect glucose in human blood and urine samples. Fresh human blood and urine samples were first analyzed in a local hospital (the fourth hospital of Changsha City) by the spectrophotometric method. Then the samples were assayed with the biosensor. A rapid and stable amperometric response was acquired at −0.25 V with the addition of 0.2 ml of sample into 5 ml of PBS. The contents of glucose in blood and urine can be calculated from the calibration curve. The recovery was tested, and the results are listed in Table 1. The good recoveries indicated that the determination of uric acid using UOx–T–GOs coated on GC was effective and sensitive.

4. Conclusions

A one-step, wet-chemical strategy for the rapid preparation of thionine–graphene oxide hybrid nanosheets was demonstrated. The proposed method was unique in its simplicity. The resulting T–GOs were used as advanced electrode materials and extensively investigated by various characterization methods, including AFM, TEM, XPS, UV, and electrochemistry. The new composite material combines the unique and attractive electrocatalytic behavior of thionine with good electronic and biocompatible properties of GOs. On the basis of these unique properties of the new material, we developed a novel assay for UA detection. The biosensor exhibited a fast response, a broad linear range, a low detection limit with satisfactory stability and repeatability and would have great potential application in determination of UA. These desirable biosensor performances are attributed to the open architectures of the T–GOs, the large surface area of GOs for enzyme immobilization, fast mass transport due to the large interlayer distance of the hybrid nanosheets, high conductivity and good biocompatibility of graphene oxide, and the synergistic catalytic effect between thionine and graphene oxide. The fabrication method of the biosensor has many advantages such as ease of fabrication, enhanced electrocatalysis, efficiently preserving the activity of enzyme molecules, and effective discrimination to the common interfering species. This study suggests that the developed strategy of tethering redox active mediator into GOs may pave the way in developing new solid support-enzyme nanohybrides for the fabrication of biosensors, energy conversion, biomedical, and other electronic systems.

Acknowledgments

This work was supported by the National Natural Science Foundation of China (no. 21105126) and the China Postdoctoral Science Foundation (nos. 2011M500126 and 2012T50656).

References

[1] U.M. Khosla, S. Zharikov, J.L. Finch, T. Nakagawa, C. Roncal, W. Mu, K. Krotova, E.R. Block, S. Prabhakar, R.J. Johnson, Kidney Int. 67 (2005) 1739–1742.
[2] J.F. Baker, E. Krishnan, L. Chen, H.R. Schumacher, Am. J. Med. 118 (2005) 816–826.
[3] H.J. Moallem, G. Taningo, C.K. Jiang, R. Hirschhorn, S. Fikrig, Clin. Immunol. 105 (2002) 75–80.
[4] E. Moor, R. Kohen, R.J. Reiter, E. Shohami, Neurosci. Lett. 316 (2001) 169–172.
[5] S. Burkhardt, R.J. Reiter, D.X. Tan, R. Hardeland, J. Cabrera, M. Karbownik, Int. J. Biochem. Cell Biol. 3 (2001) 775–783.
[6] F.J. Nieto, C. Iribarren, M.D. Gross, G.W. Comstock, R.G. Cutler, Atherosclerosis 148 (2000) 131–139.
[7] J. Dong, Y. Hu, S. Zhu, J. Xu, Y. Xu, Anal. Bioanal. Chem. 396 (2010) 1755–1762.
[8] Y. Wang, Y. Hasebe, J. Pharm. Biomed. Anal. 57 (2012) 125–132.
[9] T. Nakaminami, S.-i. Ito, S. Kuwabata, H. Yoneyama, Anal. Chem. 71 (1999) 1928–1934.
[10] C.L. Sun, H.H. Lee, J.M. Yang, C.C. Wu, Biosens. Bioelectron. 26 (2011) 3450–3455.
[11] Y.Q. Zhang, W.D. Shen, R.A. Gu, J. Zhu, R.Y. Xue, Anal. Chim. Acta 369 (1998) 123–128.
[12] Y.C. Luo, J.S. Do, C.C. Liu, Biosens. Bioelectron. 22 (2006) 482–488.
[13] Y. Zhang, G. Wen, Y. Zhou, S. Shuang, C. Dong, M.M.F. Choi, Biosens. Bioelectron. 22 (2007) 1791–1797.
[14] F. Zhang, C. Li, X. Li, X. Wang, Q. Wan, Y. Xian, L. Jin, K. Yamamoto, Talanta 68 (2006) 1353–1358.
[15] F. Zhang, X. Wang, S. Ai, Z. Sun, Q. Wan, Z. Zhu, Y. Xian, L. Jin, K. Yamamoto, Anal. Chim. Acta 519 (2004) 155–160.
[16] S.M. Usman Ali, N.H. Alvi, Z. Ibupoto, O. Nur, M. Willander, B. Danielsson, Sens. Actuators B 152 (2011) 241–247.
[17] D. Chen, Q. Wang, J. Jin, P. Wu, H. Wang, S. Yu, H. Zhang, C. Cai, Anal. Chem. 82 (2010) 2448–2455.
[18] R. Rawal, S. Chawla, N. Chauhan, T. Dahiya, C.S. Pundir, Int. J. Biol. Macromol. 50 (2012) 112–118.
[19] S. Guo, E. Wang, Acc. Chem. Res. 44 (2011) 491–500.
[20] M.S. Mauter, M. Elimelech, Environ. Sci. Technol. 42 (2008) 5843–5859.
[21] K. Welsher, S.P. Sherlock, H. Dai, Proc. Natl. Acad. Sci. U.S.A. 108 (2011) 8943–8948.
[22] S. Sorgenfrei, C.Y. Chiu, R.L. Gonzalez, Y.J. Yu, P. Kim, C. Nuckolls, K.L. Shepard, Nat. Nano 6 (2011) 126–130.
[23] S. Celebi, T.A. Nijhuis, J. van der Schaaf, F.A. de Bruijn, J.C. Schouten, Carbon 49 (2011) 501–507.
[24] T.L. Kelly, T. Gao, M.J. Sailor, Adv. Mater. 23 (2011) 1688.
[25] K. Kwon, Y.J. Sa, J.Y. Cheon, S.H. Joo, Langmuir 28 (2011) 991–996.
[26] H. Qin, P. Gao, F. Wang, L. Zhao, J. Zhu, A. Wang, T. Zhang, R.a. Wu, H. Zou, Angew. Chem. Int. Ed. 50 (2011) 12218–12221.
[27] E. Miyako, T. Deguchi, Y. Nakajima, M. Yudasaka, Y. Hagihara, M. Horie, M. Shichiri, Y. Higuchi, F. Yamashita, M. Hashida, Y. Shigeri, Y. Yoshida, S. Iijima, Proc. Natl. Acad. Sci. U.S.A. 109 (2012) 7523–7528.
[28] A. Izadi-Najafabadi, T. Yamada, D.N. Futaba, M. Yudasaka, H. Takagi, H. Hatori, S. Iijima, K. Hata, ACS Nano 5 (2011) 811–819.
[29] Y. Zhu, S. Murali, W. Cai, X. Li, J.W. Suk, J.R. Potts, R.S. Ruoff, Adv. Mater. 22 (2010) 3906–3924.
[30] O.C. Compton, S.T. Nguyen, Small 6 (2010) 711–723.
[31] D.A. Dikin, S. Stankovich, E.J. Zimney, R.D. Piner, G.H.B. Dommett, G. Evmenenko, S.T. Nguyen, R.S. Ruoff, Nature 448 (2007) 457–460.

[32] J. Zhao, G. Chen, W. Zhang, P. Li, L. Wang, Q. Yue, H. Wang, R. Dong, X. Yan, J. Liu, Anal. Chem. 83 (2011) 9100–9106.
[33] F. Li, M. Xue, X. Ma, M. Zhang, T. Cao, Anal. Chem. 83 (2011) 6426–6430.
[34] G. Eda, G. Fanchini, M. Chhowalla, Nat. Nano 3 (2008) 270–274.
[35] X. Zuo, S. He, D. Li, C. Peng, Q. Huang, S. Song, C. Fan, Langmuir 26 (2009) 1936–1939.
[36] Y. Ohno, K. Maehashi, K. Matsumoto, J. Am. Chem. Soc. 132 (2010) 18012–18013.
[37] S. Mao, G. Lu, K. Yu, Z. Bo, J. Chen, Adv. Mater. 22 (2010) 3521–3526.
[38] N. Mohanty, V. Berry, Nano Lett. 8 (2008) 4469–4476.
[39] Y. Ohno, K. Maehashi, Y. Yamashiro, K. Matsumoto, Nano Lett. 9 (2009) 3318–3322.
[40] C. Shan, H. Yang, J. Song, D. Han, A. Ivaska, L. Niu, Anal. Chem. 81 (2009) 2378–2382.
[41] Z. Wang, X. Zhou, J. Zhang, F. Boey, H. Zhang, J. Phys. Chem. C 113 (2009) 14071–14075.
[42] M. Li, S. Xu, M. Tang, L. Liu, F. Gao, Y. Wang, Electrochim. Acta 56 (2011) 1144–1149.
[43] Q. Zeng, J. Cheng, L. Tang, X. Liu, Y. Liu, J. Li, J. Jiang, Adv. Funct. Mater. 20 (2010) 3366–3372.
[44] F. Zhang, B. Zheng, J. Zhang, X. Huang, H. Liu, S. Guo, J. Zhang, Phys. Chem. C 114 (2010) 8469–8473.
[45] Q. Gao, X. Cui, F. Yang, Y. Ma, X. Yang, Biosens. Bioelectron. 19 (2003) 277–282.
[46] M. Zhou, S. Dong, Acc. Chem. Res. 44 (2011) 1232–1243.
[47] M. Zhou, Y. Zhai, S. Dong, Anal. Chem. 81 (2009) 5603–5613.
[48] Y. Guo, L. Deng, J. Li, S. Guo, E. Wang, S. Dong, ACS Nano 5 (2011) 1282–1290.
[49] M. Portaccio, D. Di Tuoro, F. Arduini, M. Lepore, D.G. Mita, N. Diano, L. Mita, D. Moscone, Biosens. Bioelectron. 25 (2010) 2003–2008.
[50] S. Baskar, J.-L. Chang, J.-M. Zen, Biosens. Bioelectron. 33 (2012) 95–99.
[51] D.R. Shobha Jeykumari, S. Ramaprabhu, S. Sriman Narayanan, Carbon 45 (2007) 1340–1353.
[52] R. Yang, C. Ruan, W. Dai, J. Deng, J. Kong, Electrochim. Acta 44 (1999) 1585–1596.
[53] Y. Xiao, H.X. Ju, H.Y. Chen, Anal. Chim. Acta 391 (1999) 299–306.
[54] M. Zhang, W. Gorski, J. Am. Chem. Soc. 127 (2005) 2058–2059.
[55] J. Li, J.D. Qiu, J.J. Xu, H.Y. Chen, X.H. Xia, Adv. Funct. Mater. 17 (2007) 1574–1580.
[56] L. Deng, Y. Liu, G. Yang, L. Shang, D. Wen, F. Wang, Z. Xu, S. Dong, Biomacromolecules 8 (2007) 2063–2071.
[57] S. Behera, C.R. Raj, Biosens. Bioelectron. 23 (2007) 556–561.